American College of Neuropsychopharmacology

www.nature.com/npp

ARTICLE

Check for updates

A preliminary study of the effects of an antimuscarinic agent on anxious behaviors and white matter microarchitecture in nonhuman primates

Nakul Aggarwal[1]✉, Jonathan A. Oler[1], Do P. M. Tromp[1], Patrick H. Roseboom[1], Marissa K. Riedel[1], Victoria R. Elam[1], Melissa A. Brotman[2] and Ned H. Kalin[1]

Myelination subserves efficient neuronal communication, and alterations in white matter (WM) microstructure have been implicated in numerous psychiatric disorders, including pathological anxiety. Recent work in rodents suggests that muscarinic antagonists may enhance myelination with behavioral benefits; however, the neural and behavioral effects of muscarinic antagonists have yet to be explored in non-human primates (NHP). Here, as a potentially translatable therapeutic strategy for human pathological anxiety, we present data from a first-in-primate study exploring the effects of the muscarinic receptor antagonist solifenacin on anxious behaviors and WM microstructure. 12 preadolescent rhesus macaques (6 vehicle control, 6 experimental; 8F, 4M) were included in a pre-test/post-test between-group study design. The experimental group received solifenacin succinate for ~60 days. Subjects underwent pre- and post-assessments of: 1) anxious temperament (AT)-related behaviors in the potentially threatening no-eye-contact (NEC) paradigm (30-min); and 2) WM and regional brain metabolism imaging metrics, including diffusion tensor imaging (DTI), quantitative relaxometry (QR), and FDG-PET. In relation to anxiety-related behaviors expressed during the NEC, significant Group (vehicle control vs. solifenacin) by Session (pre vs. post) interactions were found for freezing, cooing, and locomotion. Compared to vehicle controls, solifenacin-treated subjects exhibited effects consistent with reduced anxiety, specifically decreased freezing duration, increased locomotion duration, and increased cooing frequency. Furthermore, the Group-by-Session-by-Sex interaction indicated that these effects occurred predominantly in the males. Exploratory whole-brain voxelwise analyses of post-minus-pre differences in DTI, QR, and FDG-PET metrics revealed some solifenacin-related changes in WM microstructure and brain metabolism. These findings in NHPs support the further investigation of the utility of antimuscarinic agents in targeting WM microstructure as a means to treat pathological anxiety.

Neuropsychopharmacology (2024) 49:405–413; https://doi.org/10.1038/s41386-023-01686-1

INTRODUCTION

Anxiety disorders (ADs) affect one in three individuals at some point in their lives and are a source of significant disability, representing a major public health concern [1–4]. While selective serotonin reuptake inhibitors, benzodiazepines, and cognitive behavioral therapy are effective treatments [5], many patients are either unresponsive, have intolerable side effects, or have recurrent symptoms [6–8]. Studies in nonhuman primate (NHP) models of anxiety afford the opportunity to understand mechanisms underlying pathological anxiety and to develop novel treatment strategies that are directly translatable to humans. Our work has focused on pathological anxiety during the preadolescent period, as this is a time of rapid brain development during which ADs emerge [9–11]. Additionally, our work in preadolescent children with ADs has demonstrated alterations in WM microstructure in WM tracts linking prefrontal cortical regions with limbic structures implicated in the expression of anxiety [12, 13]. Therefore, interventions targeting critical pathophysiological processes during the preadolescent period have the potential to fundamentally change the lifelong clinical trajectory of children with ADs.

Studies characterizing white matter (WM) alterations in humans with psychopathology, including ADs, and in NHP models of anxiety suggest the possibility that WM pathways are involved in mediating pathophysiological processes. WM, which is comprised of the myelin sheaths enveloping neuronal axons, plays a central role in facilitating efficient neuronal communication and the fine-tuning of neural circuit function [14, 15]. WM-focused neuroimaging techniques, such as diffusion tensor imaging (DTI) and quantitative relaxometry (QR), are sensitive to myelination, as well as other biophysical properties underlying WM microstructure [16–20]. In turn, several neuroimaging studies have linked alterations in the WM integrity of specific WM tracts to pathological anxiety [21–25]. Our laboratory, studying youth with ADs and young anxious NHPs, has identified anxiety-related WM microstructural alterations, and these deficits appear to be more robust in boys compared to girls [13, 26]. Because of the role of WM in neuronal signaling, targeting

[1]Department of Psychiatry, University of Wisconsin-Madison, Madison, WI 53719, USA. [2]Neuroscience and Novel Therapeutics Unit, National Institute of Mental Health, Bethesda, MD 20892, USA. ✉email: naggarwal5@wisc.edu

Received: 26 December 2022 Revised: 17 July 2023 Accepted: 21 July 2023
Published online: 29 July 2023

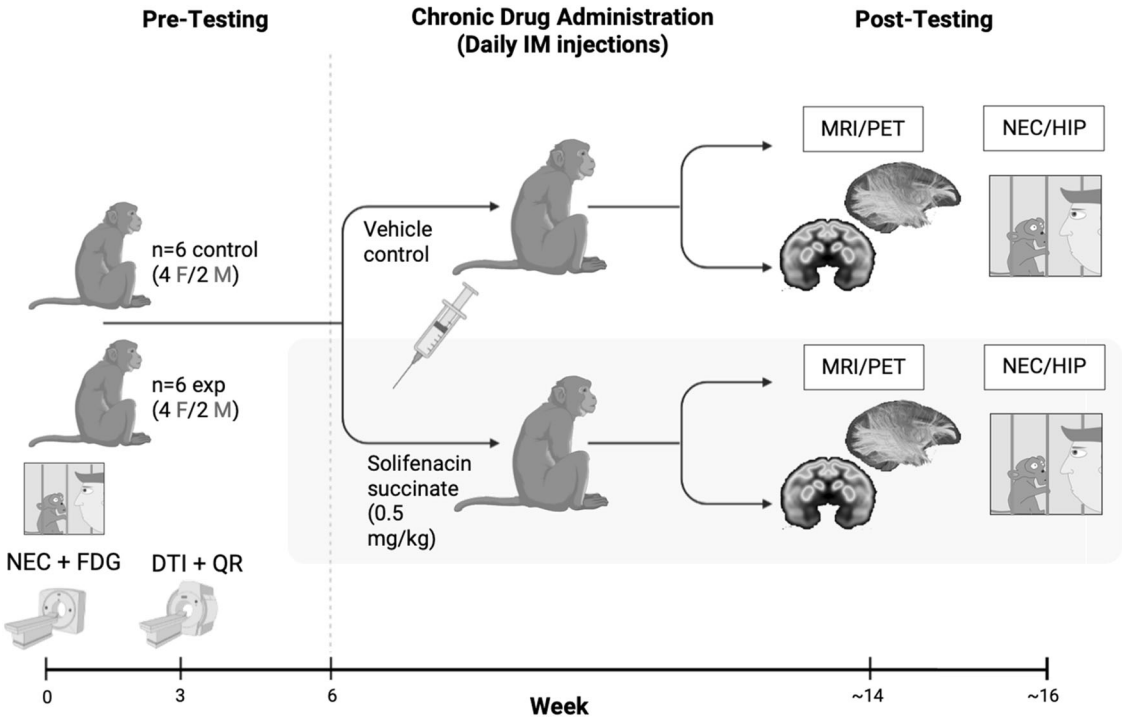

Fig. 1 Schematic of the experimental design and timeline. 12 NHPs (6 vehicle control, 6 experimental) were included in the study. All subjects underwent pre-testing, including HIP, 30-min NEC, post-NEC FDG-PET and multimodal MRI (i.e., DTI and QR). Control and experimental animals received daily vehicle or solifenacin IM injections. While still on-drug, all subjects then underwent post-testing comprised of the same behavioral and imaging components completed in pre-testing. Post-testing imaging (including MRI and PET) was performed, on average, after 59 days of treatment. Post-testing imaging was followed chronologically by post-testing behavioral assays (NEC/HIP), which were performed, on average, 22 days later, or after 71 days of treatment. Figure was created in part using BioRender.com and contains portions adapted from ref. [79].

WM pathways involved in anxiety regulation may provide a novel treatment approach for individuals with ADs.

WM is highly plastic, particularly during early development and childhood, and is sensitive to environmental factors, behavioral changes, and pharmacological agents [10, 27–31]. Recent research has highlighted muscarinic acetylcholine receptor antagonism as a potential means by which WM can be modulated [32–34]. Multiple rodent studies have reported that the systemic administration of antimuscarinic agents, including clemastine and solifenacin, leads to enhanced oligodendrocyte progenitor cell (OPC) differentiation, accelerated myelination, and reduced axonal loss in response to injury [31–33, 35–37]. A number of these studies in rodents have linked the antimuscarinic-associated changes in WM with improvements in social behaviors [31, 35, 37]. A clinical trial in multiple sclerosis (MS) patients found that clemastine treatment decreased the latency of visual-evoked potentials, but neuroimaging studies in these patients did not reveal an effect on WM [38]. At a more basic level, two studies have examined muscarinic receptor signaling in relation to human OPC differentiation. These studies, using in vivo xenoplanting and in vitro approaches, specifically implicate the M_3R muscarinic receptor in promoting human OPC differentiation [32, 33].

To examine the possibility of targeting WM as a treatment for ADs, here, in rhesus monkeys, we use a highly validated NHP model of anxious temperament to investigate the effects of solifenacin on anxiety-related behaviors and WM microarchitecture. Solifenacin is a selective M_3R muscarinic receptor antagonist that has been approved by the Food and Drug Administration (FDA) for treatment of bladder control [39]. Specifically, we use a within-subject (pre-test/post-test) and between-group (vehicle control vs. solifenacin) design to characterize the impact of chronic solifenacin treatment on anxiety-related behaviors expressed in the no-eye-contact (NEC) condition of the Human Intruder Paradigm (HIP), WM microarchitecture as assessed by DTI and QR, and threat-related regional brain metabolism.

MATERIALS AND METHODS

Subjects and housing

Rhesus macaques underwent behavioral screening for potential inclusion in the study. Specifically, potential subjects were exposed to 10 min of the no-eye-contact (NEC) condition of the human intruder paradigm (HIP), a highly validated behavioral task designed to elicit anxious responses in NHPs [40, 41]. As in humans, anxiety in NHPs is dimensional and individuals expressing high levels of behavioral inhibition are considered to be in the pathological range [42–46]. Because of our interest in the anti-anxiety effects of solifenacin and the dimensional nature of anxiety, we selected animals with mid-to-high levels of behavioral inhibition (i.e., freezing) for this study.

Eight female and four male rhesus monkeys (mean (±s.d.) age = 2.00 (± 0.23) years) were included in the study and grouped into cage-mate pairs (vehicle control vs. solifenacin). Animal weights are provided in Supplementary Table 7. Animals were cared for and housed at the Wisconsin National Primate Research Center (WNPRC) and the Harlow Center for Biological Psychology. Standard husbandry included a 12-h light/dark cycle, two daily feeding sessions, ad libitum access to water, and daily enrichment. All procedures were performed according to the federal guidelines of animal care and use and with the approval of the University of Wisconsin-Madison Institutional Animal Care and Use Committee.

Experimental timeline and drug administration

12 preadolescent rhesus macaques (6 vehicle control, 6 experimental; 8F, 4M) were included in a pre-test/post-test control group study design (Fig. 1). All subjects underwent pre-drug MRI imaging, PET imaging, and behavioral testing. MRI imaging and behavioral testing was performed on average 22 days (range: 6–55) prior to drug administration; PET imaging was performed on average 42 days (range: 20–78) prior to drug administration. Subjects received either daily solifenacin or vehicle injections and then, while

still on-drug, at 59 days on average (range: 54–64), PET and MRI imaging was performed on all subjects. At an average of 71 days (range: 69–75), again while still on-drug, behavioral testing was performed on all subjects. The experimental group received solifenacin succinate (0.5 mg/kg IM) (Toronto Research Chemicals); the control group received vehicle (0.25 ml/kg of 10% dimethyl sulfoxide [DMSO] in 0.9% saline IM). We selected the dose of 0.5 mg/kg of solifenacin per day based on dosages used in rodent studies, general guidelines for adapting rodent dosing to primates, and dose ranges approved in humans to treat urinary incontinence [32, 39, 47, 48].

Human Intruder Paradigm (HIP) and the No-Eye-Contact (NEC) condition

The Human Intruder Paradigm (HIP) assesses monkeys in three different contexts eliciting different defensive responses. The HIP begins with the Alone (AL) condition, during which a monkey is separated from its cage-mate and is placed into a test cage by itself. This context typically elicits separation behaviors such as coo-vocalizations and increases in locomotion. The Alone condition is followed by the No-Eye-Contact (NEC) condition, wherein a human intruder enters the room and presents her/his profile to the monkey, while avoiding direct eye contact. Responses to this potentially threatening situation include increases in freezing, decreases in locomotion, and decreases in coo vocalizations. The final context is the Stare (ST) condition, during which the intruder reenters the room and stares directly at the monkey, eliciting hostile behaviors directed toward the intruder (i.e., bark vocalizations and experimenter-directed hostility). The full HIP paradigm lasts 50 min, consisting of 30 min of the AL condition, 10 min of the NEC condition, and 10 min of the ST condition.

Responses in the NEC condition, which elicits behavioral inhibition, are used to quantify anxious temperament (AT). More specifically, two behavioral responses (increased freezing and decreased cooing) and a physiological stress response (heightened plasma cortisol) are combined to calculate a composite AT score for each monkey [49]. Because of the importance of the NEC in assessing AT, in addition to the HIP, subjects underwent an additional behavioral testing session, consisting of 30 min of only the NEC. In summary, all subjects underwent pre- and post-behavioral testing consisting of both: 1) the full HIP paradigm (30 min AL; 10 min NEC; 10 min ST), completed pre- and post-drug; and 2) a separate behavioral testing session comprised of 30 min of the NEC, completed pre- and post-drug.

Cortisol assay

Plasma samples, collected after the 30-min NEC test, were assayed for cortisol in duplicate using the MP Biomedicals (Solon, OH, USA) Immuchem coated tube radioimmunoassay. The intra-assay CV percentage was 4.9 and the inter-assay CV percentage was 9.9. The detection limit defined by the lowest standard was 1 mg/dL. Prior to analysis, cortisol values were residualized for the time of day at which they were collected.

MRI acquisition and data processing

Subjects were imaged with a 3T MR750 scanner (GE Healthcare, Waukesha, WI) pre- and post-drug (vehicle or solifenacin). Whole brain, 3D T1-weighted images were acquired with MPnRAGE [50, 51], an MRI sequence that enables quantitative relaxometry (QR) analysis, with 0.625 mm isotropic spatial resolution, reconstructed to 0.47 mm isotropic resolution; TE = 2.3 ms and TR = 6.1 ms. A 2D echo-planar, spin-echo, single-shell DTI sequence was acquired with the following parameters: TR/TE = 7000/65.8 ms, flip angle = 90°, NEX = 1, FOV = 125 mm, acquisition matrix = 128 × 128 with 0.625 partial Fourier encoding, reconstructed in-plane spatial resolution of 0.4883 mm × 0.4883 mm and a slice thickness/gap = 1.3/0 mm, 64 interleaved slices, echo-planar spacing = 884 µs, ASSET parallel imaging ($R = 2$), $b = 1000$ s/mm^2, 72 non-colinear gradient directions (i.e., b-vectors, with each gradient direction/b-vector consisting of three separate vectors [x, y, z]), six non-diffusion weighted images. In addition, co-planar external field maps were obtained using a dual-echo gradient echo sequence with TE1 = 7 ms and TE2 = 10 ms.

In each scanning session, subjects were weighed and then sedated with ketamine (15 mg/kg, IM) and dexdomitor (15 µg/kg, IM). The monkeys were then placed into a custom built eight-channel receive array for NHP imaging with a built-in stereotaxic frame (Clinical MR Solutions). Vital signs, including heart rate, oxygen saturation, end tidal CO_2, respiration rate and body temperature, were monitored throughout the scan. Following conclusion of the scan, sedation was reversed with atipamezole (150 µg/kg, IM).

The structural MPnRAGE images for each subject were skull-stripped and then iteratively spatially normalized with non-linear, diffeomorphic registration using Advanced Normalization Tools (ANTs) software [52] to produce a population T1-template. The population study T1-template was then warped to a 592-monkey T1-template [42]. The spatial transformations generated from: 1) the construction of the population T1-template for each scan, and 2) the population T1-template to 592 T1-template registration were then sequentially applied to warp the corresponding subject T1 images into 592-monkey template space. Next, longitudinal relaxation rate (qR_1) maps were generated from subject T1 images now in 592-monkey space. Finally, in 592-space, qR_1 images were smoothed with a 4-mm FWHM Gaussian kernel.

DTI scans were processed as described in our previous work [26, 27]. Briefly, images were corrected for field inhomogeneities, noise, Gibbs ringing, and eddy currents, after which the tensors were calculated using a robust tensor estimation in Camino [53]. Tensor images were co-registered iteratively using non-linear tensor-based normalization tools (DTI-TK [54]), and then registered to the 592-monkey T1-template. In 592-space, prototypical DTI parameter maps of fractional anisotropy (FA), mean diffusivity (MD), radial diffusivity (RD), and axial diffusivity (XD) were calculated. All DTI parameter maps were smoothed with a 4-mm FWHM Gaussian kernel.

PET acquisition and data processing—NEC-FDG

Subjects underwent FDG-PET imaging following the 30-min NEC tests in the pre- and post-drug sessions. To measure threat-related metabolic brain activity, animals were briefly restrained, intravenously injected with FDG (~7.0 mCi), and then placed in a test cage for 30 min, during which time the animals were exposed to the NEC. After the 30-min FDG uptake period, animals were anesthetized with ketamine (15 mg/kg, IM), given atropine sulfate (0.04 mg/kg, IM), and then fitted with an endotracheal tube and induced and maintained on isofluorane (typically less than 2% isoflurane/O_2) anesthesia throughout the scanning procedure. Vital signs, including heart rate, oxygen saturation, end tidal CO_2, respiration rate and body temperature, were monitored throughout the scan.

Sixty-minute emission PET scans were reconstructed using standard filtered back projection methods with attenuation- and scatter-correction into a matrix size of 128 × 128 × 95 with voxel dimensions of 0.95 mm × 0.95 mm × 0.80 mm, reflecting the integrated brain metabolism that occurred during the 30 min of FDG uptake. Native-space FDG-PET images were iteratively normalized using Advanced Normalization Tools (ANTs) software [52] to create a population PET-template. The population PET template was then registered to the 592-monkey T1-template. The spatial transformations generated from: 1) the construction of the population PET-template for each scan, and 2) the population PET-template to 592 T1-template registration were then sequentially applied to warp the corresponding subject PET images into 592-monkey template space. The normalized FDG-PET images were scaled to the whole-brain signal using [55]. PET images were spatially smoothed with a 4-mm FWHM Gaussian kernel.

Statistical analyses

Anxiety-related behaviors. Anxiety-related behaviors (freezing, locomotion, and cooing) were scored by a trained rater, who was blind to monkey group assignment. Freezing was defined as a lack of movement and vocalization for greater than 3 s. Locomotion was defined as ambulation of one or more full steps at any speed. Both were recorded in seconds per 5-min bin of the HIP or NEC session. Freezing and locomotion scores in each bin were log-transformed and converted to z-scores. Cooing was measured as the number of coo-vocalizations during each 5-min bin of HIP or NEC. Cooing frequencies in each bin were square-root transformed and converted to z-scores.

Linear mixed-effects (LME) models were built to assess each behavior of interest (freezing, locomotion, cooing). LME models are ideally suited for our pre-test/post-test design, as they take advantage of repeated measures data and enable robust estimation of within-subject effects [56]. For each behavior, LME models included Group (vehicle control vs. solifenacin), Session (pre vs. post), and Sex (female vs. male), estimating all possible interactions and main effects. In analyses of the HIP data, LME models also included Condition (AL, NEC, ST). The primary interactions of interest in all analyses were the Group-by-Session-by-Sex three-way interaction and Group-by-Session two-way interaction.

WM and brain metabolism metrics (MRI and PET). For QR, DTI, and PET analyses, pre-post difference maps were first generated for each subject (pre-drug images were subtracted from post-drug images using *fslmaths* [55]). For each modality, these difference maps were then subject to whole-brain voxelwise analyses (using *3dttest* in AFNI [57]) to test for group

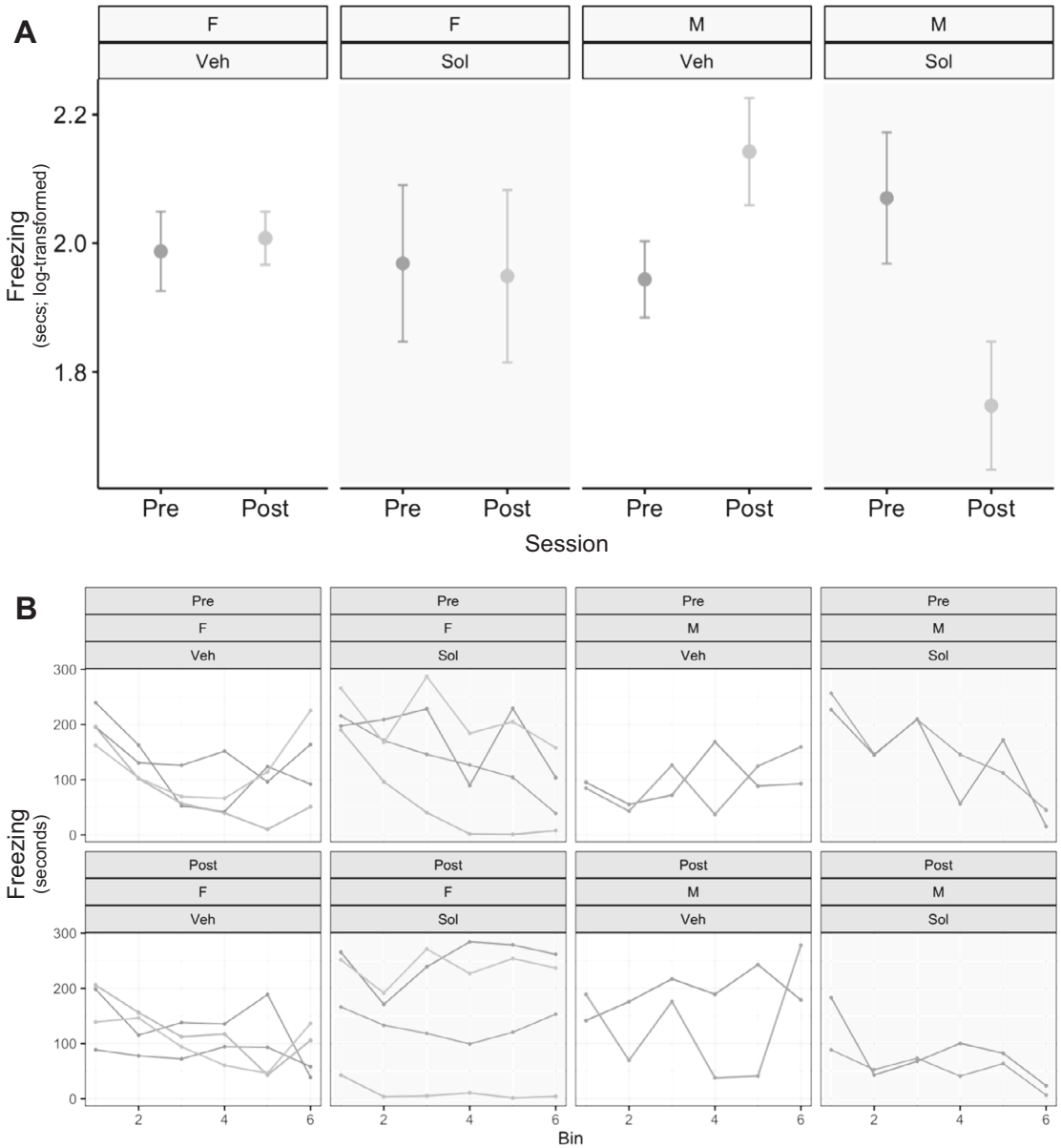

Fig. 2 Group-by-Session-by-Sex interaction in relation to freezing behavior in the 30-min NEC. A Average time spent freezing (in log-transformed seconds) across the six bins of the 30-min NEC, split by Group (Veh vs. Sol), Session (Pre vs. Post), and Sex (F vs. M). Bars represent standard (SE) error of the mean. Note a significant Group-by-Session-by-Sex interaction ($t = 2.202$, df = 128, $p = 0.029$). **B** For illustrative purposes, depiction of subject-level freezing behavior (raw seconds) across the six 5-min bins of the 30-min NEC, split by Group, Session, and Sex, where each line represents a single subject. In both panels, yellow shading denotes the solifenacin-treated animals.

differences (vehicle control vs. solifenacin) in post-minus-pre changes in imaging metrics. Analyses controlled for age at study entry. Given the exploratory nature of these analyses, results were assessed at an uncorrected threshold of $p < 0.005$ (uncorrected, two-tailed).

RESULTS

Solifenacin administration attenuates anxiety-related behaviors in the 30-min NEC condition

Using a linear mixed-effects (LME) model, we examined solifenacin-induced changes in the expression of three key anxiety-related behaviors—freezing, cooing, and locomotion. Significant Group-by-Session interactions were observed in relation to freezing, cooing, and locomotion behaviors in the 30-min NEC test. Specifically, freezing behavior ($t = -2.572$, df = 128, $p = 0.011$) was significantly reduced post-drug in the solifenacin group compared to the vehicle control group. Cooing ($t = 3.424$, df = 128, $p < 0.001$) and locomotion ($t = 4.028$, df = 128, $p < 0.001$) behaviors were significantly increased post-drug in the solifenacin group compared to the vehicle control group. Moreover, for all three behaviors of interest, significant Group-by-Session-by-Sex (three-way) interactions were also observed (freezing: $t = 2.202$, df = 128, $p = 0.029$ [Fig. 2A]; cooing: $t = -3.310$, df = 128, $p = 0.001$ [Fig. 3A]; locomotion: $t = -5.279$, df = 128, $p < 0.001$ [Supplementary Fig. 1A]), such that post-drug changes in anxiety-related behaviors in the solifenacin-treated group appeared to be specific to males. Examination of the data from the four male subjects demonstrated that anxiety-related behaviors were attenuated post-drug in both solifenacin-treated males, whereas the vehicle-treated males did not show this effect (Figs. 2B and 3B; Supplementary Fig. 1B). Threat-related cortisol was assessed immediately after NEC exposure, which was not found to

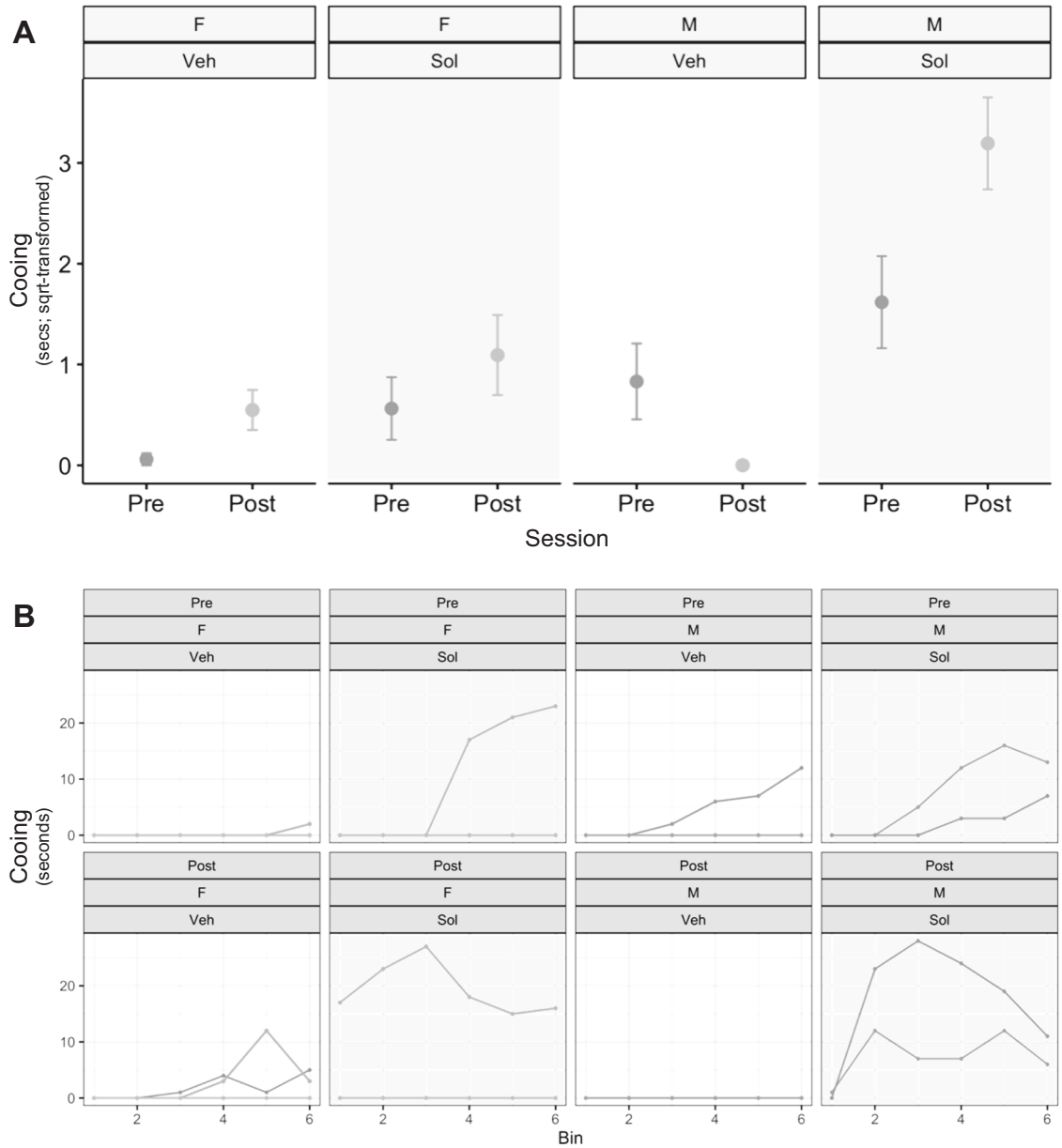

Fig. 3 Group-by-Session-by-Sex interaction in relation to cooing behavior in the 30-min NEC. A Average time spent cooing (in sqrt-transformed seconds) across the six bins of the 30-min NEC, split by Group (Veh vs. Sol), Session (Pre vs. Post), and Sex (F vs. M). Bars represent standard (SE) error of the mean. Note a significant Group-by-Session-by-Sex interaction ($t = -3.310$, df = 128, $p = 0.001$). **B** For illustrative purposes, depiction of subject-level cooing behavior (raw seconds) across the six 5-min bins of the 30-min NEC, split by Group, Session, and Sex, where each line represents a single subject. In both panels, yellow shading denotes the solifenacin-treated animals.

be affected by solifenacin treatment ($t = 0.294$, df = 8, $p = 0.776$) (Supplementary Fig. 2). Taken together, these results suggest that solifenacin treatment results in anti-anxiety like effects, predominantly in males, but that it does not impact threat-related reactivity of the pituitary-adrenal axis. However, these findings were not confirmed in the full HIP test, which differs from the 30-min NEC test in that it is limited to 10 min of NEC, and includes 30 min of AL and 10 min of ST. Specifically, no significant Group-by-Session (2-way) or Group-by-Session-by-Sex (3-way) interactions were detected in relation to freezing, cooing, or cortisol levels during the 10 min of NEC in the full HIP.

Solifenacin-induced changes in WM imaging metrics (QR and DTI)

The sample size for assessing between-group differences with imaging methods is small and therefore any findings should be cautiously interpreted. Despite the small *n*, we performed exploratory analyses reducing the statistical threshold to $p < 0.005$ as an opportunity to identify regions that might be affected by solifenacin treatment. We hypothesized that solifenacin would generally result in increased WM microstructural integrity, as indexed by QR and DTI metrics. With respect to QR, voxelwise analyses of group (vehicle control vs. solifenacin) differences in post-minus-pre images revealed small gray matter (GM) and WM clusters in which increases in qR_1 were specific to the solifenacin-treated group ($p < 0.005$, two-tailed). Regions with solifenacin-related increases in qR_1 included clusters overlapping with the GM and WM of the inferior frontal gyrus, dorsal prefrontal WM, corona radiata, external capsule, sagittal striatum, corticospinal tract, cingulum, and cerebral peduncle (Fig. 4A and Supplementary Table 1). We also observed reductions in qR_1 in several regions, including cerebellum, middle temporal gyrus, anterior

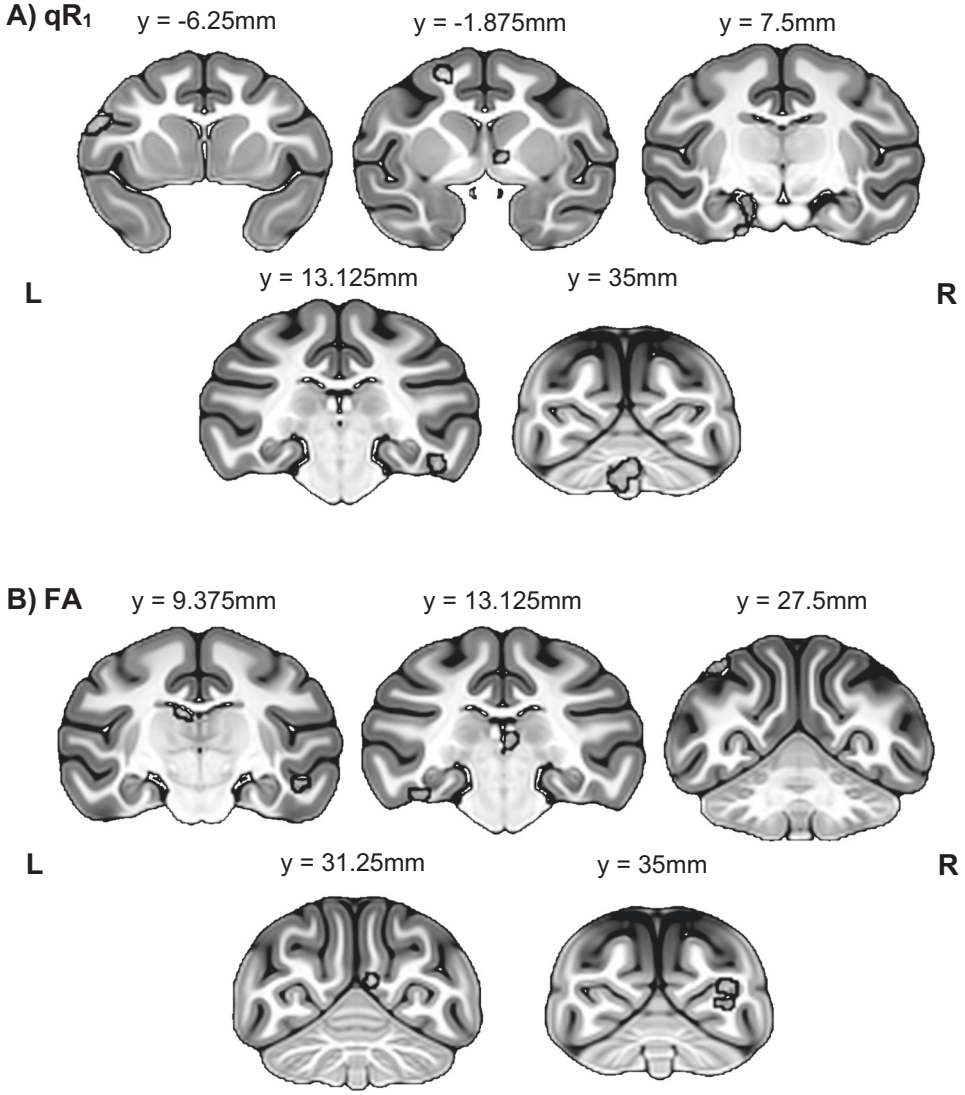

Fig. 4 Group-by-session interaction in relation to WM metrics (qR_1 and FA) in voxelwise analyses. Top five largest clusters shown for qR_1 (**A**) and FA (**B**) moving from anterior to posterior (cluster information in Supplementary Tables 1, 2). Red and blue clusters represent voxels in which solifenacin-treated animals showed relative increases or decreases in qR_1 or FA post-treatment compared to vehicle controls, respectively ($p < 0.005$). *Y*-coordinates indicate position in millimeters anterior (negative) or posterior (positive) to the anterior commissure.

commissure, and internal capsule (Fig. 4A and Supplementary Table 1). With respect to the DTI metrics, FA and RD are considered to be the most related to qR_1 [58, 59]. Solifenacin-treated animals showed increased FA in small clusters in some of the pathways in which qR_1 was increased, such as the internal capsule, as well as reductions in regions including midline thalamus and inferior temporal gyrus (Fig. 4B and Supplementary Table 3). In addition, the solifenacin-treated group demonstrated increased XD in multiple WM regions, including in small clusters overlapping with inferior frontal gyrus, and reduced XD in somatosensory cortex (Supplementary Fig. 3 and Supplementary Table 2). Full voxelwise results, including MD and RD data, can be found in Supplementary Tables 4, 5 and Supplementary Figs. 4, 5.

Solifenacin-induced changes in regional brain metabolism (FDG-PET)

Voxelwise analyses of group (vehicle control vs. solifenacin) differences in post-minus-pre FDG-PET images revealed threat-related decreases in metabolism in the solifenacin-treated group in small clusters overlapping with the bilateral orbitofrontal cortex and middle temporal gyrus ($p < 0.005$, uncorrected), which are regions implicated in the neural circuitry underlying AT in NHPs and ADs in humans. Solifenacin-related increases in metabolism were detected in the occipital cortex (Fig. 5 and Supplementary Table 6).

DISCUSSION

This study characterized the impacts of solifenacin, an FDA-approved M_3R muscarinic antagonist, on anxiety-related behaviors, WM microstructure, and threat-related regional brain metabolism in rhesus monkeys. To the best of our knowledge, this is the first study to assess the effects of an antimuscarinic agent in a NHP model relevant to pathological anxiety. We report preliminary evidence to suggest that solifenacin treatment may attenuate anxiety-related behaviors in NHPs and that this effect may be specific to males. The WM imaging data revealed small clusters in distinct regions in which solifenacin appeared to increase or decrease WM microstructural integrity. Similarly, increases and decreases in regional brain metabolism were observed in relation to solifenacin treatment. Because of the small sample size, caution should be used in interpreting the results of this experiment, especially in relation to the imaging data.

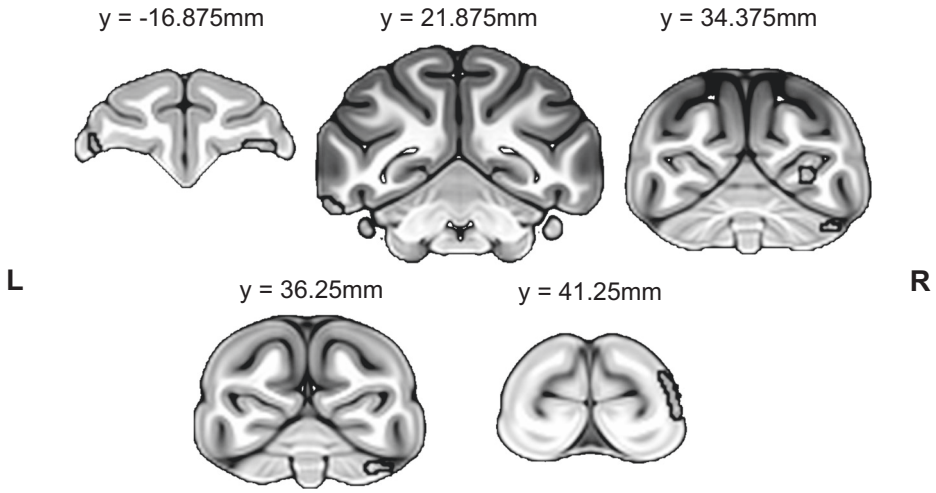

Fig. 5 Group-by-Session interaction in relation to FDG in voxelwise analyses. Top five largest clusters shown, moving from anterior to posterior (cluster information in Supplementary Table 6). Red and blue clusters represent voxels in which solifenacin-treated animals showed relative increases or decreases in FDG metabolism post-treatment compared to vehicle controls, respectively ($p < 0.005$). *Y*-coordinates indicate position in millimeters anterior (negative) or posterior (positive) to the anterior commissure.

The preclinical rationale for this study is based on work that links muscarinic antagonism to oligodendrocyte progenitor cell (OPC) differentiation and myelination. OPCs are critical to the process of myelinogenesis, as they differentiate into mature oligodendrocytes that proceed to myelinate axons, facilitating efficient neuronal signal transfer [60, 61]. Importantly, OPCs are present in the brain throughout the lifespan and orchestrate new myelin formation not only in early development but also adulthood [62–65]. Studies performed in rodent models demonstrated that systemic anti-muscarinic treatment, most commonly clemastine, a relatively nonselective muscarinic antagonist, stimulated OPC differentiation and promoted new myelin formation [31, 32, 36, 37]. Some of these studies also demonstrated that clemastine-induced OPC and myelin changes were associated with reductions in social avoidance and enhanced remote memory recall [31, 35, 37]. One study particularly relevant to humans was performed by xenoplanting human OPCs into hypomyelinated mice, demonstrating that solifenacin, an M_3R-specific muscarinic antagonist, promoted human OPC differentiation [32]. Another study found that M_3R knockdown enhanced human OPC differentiation in vitro, in addition to promoting remyelination by xenoplanted human OPCs in hypomyelinated mice, providing further support for a role of the M_3R receptor in mediating human OPC function [33].

Our study provides evidence for an anti-anxiety effect of solifenacin, as solifenacin-treated animals exhibited significantly decreased freezing, increased cooing, and increased locomotion during the 30-min of NEC. These behavioral effects appeared to predominantly occur in males. Similar solifenacin-related behavioral changes were not observed in response to the full HIP, which, compared to the 30-min NEC, has a shorter 10-min NEC period, interspersed with 10 min of ST and three 10-min AL periods. We speculate that the discrepancy in the findings may be due to the monkeys' differential experiences in relation to these two paradigms. It is also possible that the behavioral effects found in the 30-min NEC paradigm were evident because of the extended length of NEC exposure, which enabled considerably more observations.

Exploratory quantitative relaxometry and DTI analyses suggested solifenacin-related increases, as well as decreases, in WM microstructural metrics in several WM and GM regions across the brain, indexed by small clusters of voxels showing altered qR_1, XD, or FA. To the best of our knowledge, only one other study has investigated pre-post changes in WM imaging in relation to antimuscarinic treatment, finding no changes in WM metrics in multiple sclerosis (MS) patients in response to clemastine treatment [38]. We highlight our results from the quantitative relaxometry analyses, as QR metrics, including the longitudinal relaxation rate (qR_1), are derived from the MPnRAGE MRI sequence, a high-resolution T1 imaging technique that is highly sensitive to the presence of lipid molecules in brain tissue and, therefore, thought to be a reliable marker of myelination [19, 66, 67]. We emphasize that DTI and QR metrics, while sensitive to myelination, are not specific to myelination processes, as they can reflect other biophysical properties, including axon caliber, fiber density, and cellular density [16–20]. The results indicate small solifenacin-induced increases in qR_1 in a distributed network of WM pathways. To the extent that these are reflective of changes in myelination, based on other preclinical work, one possibility is that these effects could be due to solifenacin-induced OPC differentiation and increased myelination [32]. With respect to the DTI results, solifenacin-induced increases in XD and FA may reflect enhanced axonal integrity and coherence [68–70]. In relation to FDG-PET analyses, we observed decreased glucose metabolism in regions of the OFC following solifenacin treatment. These changes might be expected given our previous work in NHPs, which links heightened metabolism in these prefrontal regions to higher levels of anxiety [42, 71]. We emphasize that these results are preliminary and that we also found changes representative of WM microstructure and glucose metabolism in opposite of the predicted directions.

While we believe that the anti-anxiety effects observed in this study are due to the effects of solifenacin on WM microstructure, it is also possible that solifenacin could affect behavior through other mechanisms. For example, earlier work in humans reported that the acute administration of an antimuscarinic agent (scopolamine) led to reductions in anxiety and depressive symptoms [72]. In preclinical studies, using anticholinergic agents or knockdown of the M_3R receptor, mixed effects on locomotion have been reported [31, 73–75]. In our study, solifenacin administration was associated with increases in locomotion during threat exposure, which, along with a reduction in freezing, we interpreted to reflect decreased anxiety.

The sex-specific nature of the solifenacin-related reductions in anxious behaviors observed in the 30-min NEC test is intriguing and is particularly interesting in the context of our previous work. Our laboratory has shown that WM alterations in both youth with ADs and in highly anxious NHPs appear to be sexually dimorphic, with more robust anxiety-related decreases in WM microstructural integrity occurring in males [12, 13, 26]. The reason for the male-specific behavioral effects observed in the current study remains

unclear. While we found overall effects of solifenacin on WM microstructure and regional brain metabolism, the sample size did not allow us to confidently assess sex-specific effects on these metrics. We are unaware of any other studies examining potentially sexually dimorphic effects of solifenacin on WM parameters. Along with our previous findings, the results from the current study suggest the possibility that WM microstructure in males is more sensitive to stress- and anxiety-related influences, as well as potentially to pharmacological manipulations, such as antimuscarinic agents. Some data from preclinical studies supports this notion. For example, evidence from rodent studies suggests that male OPCs may be particularly sensitive to cytotoxic stress compared to female OPCs, with higher levels of subsequent cell death [76, 77]. Relatedly, one study indicates that progesterone may serve a protective role in shielding mature oligodendrocytes from cellular stress, and that this effect may be more prominent in females than in males [78].

In summary, this study in a highly validated and translatable NHP model of anxiety is the first to examine the possibility of using an M_3R antimuscarinic agent as a treatment strategy for pathological anxiety. The results provide preliminary evidence which support further studies focused on the therapeutic potential of solifenacin and more generally on modulating WM for the treatment of ADs.

REFERENCES

1. Kessler RC, Petukhova M, Sampson NA, Zaslavsky AM, Wittchen HU. Twelve-month and lifetime prevalence and lifetime morbid risk of anxiety and mood disorders in the United States. Int J methods Psychiatr Res. 2012;21:169–84.
2. Konnopka A, König H. Economic burden of anxiety disorders: a systematic review and meta-analysis. Pharmacoeconomics. 2020;38:25–37.
3. Bandelow B, Michaelis S. Epidemiology of anxiety disorders in the 21st century. Dialogues Clin Neurosci. 2015;17:327–35.
4. Yang X, Fang Y, Chen H, Zhang T, Yin X, Man J, et al. Global, regional and national burden of anxiety disorders from 1990 to 2019: results from the Global Burden of Disease Study 2019. Epidemiol Psych Sci. 2021;30:e36.
5. Bandelow B, Michaelis S, Wedekind D. Treatment of anxiety disorders. Dialogues Clin Neurosci. 2017;19:93–107.
6. Ginsburg GS, Becker-Haimes EM, Keeton C, Kendall PC, Iyengar S, Sakolsky D, et al. Results from the child/adolescent anxiety multimodal extended long-term study (CAMELS): primary anxiety outcomes. J Am Acad Child Adolesc Psychiatry. 2018;57:471–80.
7. Ginsburg GS, Becker EM, Keeton CP, Sakolsky D, Piacentini J, Albano AM, et al. Naturalistic follow-up of youths treated for pediatric anxiety disorders. JAMA Psychiatry. 2014;71:310–8.
8. Scholten W, Have M ten, Geel C van, Balkom A van, Graaf R de, Batelaan N. Recurrence of anxiety disorders and its predictors in the general population. Psychol Med. 2023;53:1334–42.
9. Barnea-Goraly N, Menon V, Eckert M, Tamm L, Bammer R, Karchemskiy A, et al. White matter development during childhood and adolescence: a cross-sectional diffusion tensor imaging study. Cereb Cortex. 2005;15:1848–54.
10. Lebel C, Beaulieu C. Longitudinal development of human brain wiring continues from childhood into adulthood. J Neurosci. 2011;31:10937–47.
11. Costello EJ, Mustillo S, Erkanli A, Keeler G, Angold A. Prevalence and development of psychiatric disorders in childhood and adolescence. Arch Gen Psychiatry. 2003;60:837–44.
12. Aggarwal N, Williams LE, Tromp DPM, Pine DS, Kalin NH. A dynamic relation between whole-brain white matter microstructural integrity and anxiety symptoms in preadolescent females with pathological anxiety. Transl Psychiatry. 2022;12:57.
13. Tromp DPM, Williams LE, Fox AS, Oler JA, Roseboom PH, Rogers GM, et al. Altered uncinate fasciculus microstructure in childhood anxiety disorders in boys but not girls. Am J Psychiatry. 2019;176:208–16.
14. Fields RD. Myelin formation and remodeling. Cell. 2014;156:15–7.
15. Miron VE, Kuhlmann T, Antel JP. Cells of the oligodendroglial lineage, myelination, and remyelination. Biochim Biophys Acta 2011;1812:184–93.
16. Friedrich P, Fraenz C, Schlüter C, Ocklenburg S, Mädler B, Güntürkün O, et al. The relationship between axon density, myelination, and fractional anisotropy in the human corpus callosum. Cereb Cortex. 2020;30:2042–56.
17. Roberts TPL, Liu F, Kassner A, Mori S, Guha A. Fiber density index correlates with reduced fractional anisotropy in white matter of patients with glioblastoma. Am J Neuroradiol. 2005;26:2183–6.
18. Beaulieu C. The basis of anisotropic water diffusion in the nervous system—a technical review. NMR Biomed. 2002;15:435–55.
19. Lazari A, Lipp I. Can MRI measure myelin? systematic review, qualitative assessment, and meta-analysis of studies validating microstructural imaging with myelin histology. Neuroimage. 2021;230:117744.
20. Song SK, Yoshino J, Le TQ, Lin SJ, Sun SW, Cross AH, et al. Demyelination increases radial diffusivity in corpus callosum of mouse brain. Neuroimage. 2005;26:132–40.
21. Tromp DPM, Grupe DW, Oathes DJ, McFarlin DR, Hernandez PJ, Kral TRA, et al. Reduced structural connectivity of a major frontolimbic pathway in generalized anxiety disorder. Arch Gen psychiatry. 2012;69:925–34.
22. Baur V, Hänggi J, Rufer M, Delsignore A, Jäncke L, Herwig U, et al. White matter alterations in social anxiety disorder. J Psychiatr Res. 2011;45:1366–72.
23. Kim MJ, Whalen PJ. The structural integrity of an amygdala-prefrontal pathway predicts trait anxiety. J Neurosci. 2009;29:11614–8.
24. Liao M, Yang F, Zhang Y, He Z, Su L, Li L. White matter abnormalities in adolescents with generalized anxiety disorder: a diffusion tensor imaging study. BMC Psychiatry. 2014;14:41.
25. Westlye LT, Bjørnebekk A, Grydeland H, Fjell AM, Walhovd KB. Linking an anxiety-related personality trait to brain white matter microstructure: diffusion tensor imaging and harm avoidance. Arch Gen Psychiatry. 2011;68:369–77.
26. Tromp DPM, Fox AS, Oler JA, Alexander AL, Kalin NH. The relationship between the uncinate fasciculus and anxious temperament is evolutionarily conserved and sexually dimorphic. Biol Psychiatry. 2019;86:890–8.
27. Aggarwal N, Moody JF, Dean IDC, Tromp DPM, Kecskemeti SR, Oler JA, et al. Spatiotemporal dynamics of nonhuman primate white matter development during the first year of life. Neuroimage. 2021;231:117825.
28. Dimond D, Rohr CS, Smith RE, Dhollander T, Cho I, Lebel C, et al. Early childhood development of white matter fiber density and morphology. Neuroimage. 2020;210:116552.
29. Scholz J, Klein MC, Behrens TEJ, Johansen-Berg H. Training induces changes in white-matter architecture. Nat Neurosci. 2009;12:1370–1.
30. Sampaio-Baptista C, Khrapitchev AA, Foxley S, Schlagheck T, Scholz J, Jbabdi S, et al. Motor skill learning induces changes in white matter microstructure and myelination. J Neurosci. 2013;33:19499–503.
31. Liu J, Dupree JL, Gacias M, Frawley R, Sikder T, Naik P, et al. Clemastine enhances myelination in the prefrontal cortex and rescues behavioral changes in socially isolated mice. J Neurosci. 2016;36:957–62.
32. Abiraman K, Pol SU, O'Bara MA, Chen GD, Khaku ZM, Wang J, et al. Antimuscarinic adjunct therapy accelerates functional human oligodendrocyte repair. J Neurosci. 2015;35:3676–88.
33. Welliver RR, Polanco JJ, Seidman RA, Sinha AK, O'Bara MA, Khaku ZM, et al. Muscarinic receptor m3r signaling prevents efficient remyelination by human and mouse oligodendrocyte progenitor cells. J Neurosci. 2018;38:6921–32.
34. Fields RD, Dutta DJ, Belgrad J, Robnett M. Cholinergic signaling in myelination. Glia. 2017;65:687–98.
35. Pan S, Mayoral SR, Choi HS, Chan JR, Kheirbek MA. Preservation of a remote fear memory requires new myelin formation. Nat Neurosci. 2020;23:487–99.
36. Du W, Deng Y, Jiang R, Tong L, Li R, Jiang X. Clemastine enhances myelination, delays axonal loss and promotes functional recovery in spinal cord injury. Neurochem Res. 2022;47:503–15.
37. Li Z, He Y, Fan S, Sun B. Clemastine rescues behavioral changes and enhances remyelination in the cuprizone mouse model of demyelination. Neurosci Bull. 2015;31:617–25.
38. Green AJ, Gelfand JM, Cree BA, Bevan C, Boscardin WJ, Mei F, et al. Clemastine fumarate as a remyelinating therapy for multiple sclerosis (ReBUILD): a randomised, controlled, double-blind, crossover trial. Lancet. 2017;390:2481–9.
39. Drug Approval Package: VesiCare (Solifenacin Succinate) NDA #021518 [Internet]. Available from: https://www.accessdata.fda.gov/drugsatfda_docs/nda/2004/21-518_VesiCare.cfm. Accessed 25 Dec 2022.
40. Kalin NH, Shelton SE. Defensive behaviors in infant rhesus monkeys: environmental cues and neurochemical regulation. Science. 1989;243:1718–21.
41. Kalin NH. The neurobiology of fear. Sci Am. 1993;268:94–101.
42. Fox AS, Oler JA, Shackman AJ, Shelton SE, Raveendran M, McKay DR, et al. Intergenerational neural mediators of early-life anxious temperament. Proc Natl Acad Sci. 2015;112:9118–22.
43. Rosenbaum JF, Biederman J, Bolduc-Murphy EA, Faraone SV, Chaloff J, Hirshfeld DR, et al. Behavioral inhibition in childhood: a risk factor for anxiety disorders. Harv Rev Psychiatry. 1993;1:2–16.
44. Shackman AJ, Fox AS, Oler JA, Shelton SE, Oakes TR, Davidson RJ, et al. Heightened extended amygdala metabolism following threat characterizes the early phenotypic risk to develop anxiety-related psychopathology. Mol Psychiatry. 2017;22:724–32.
45. Goldsmith HH, Hilton EC, Phan JM, Sarkisian KL, Carroll IC, Lemery-Chalfant K, et al. Childhood inhibition predicts adolescent social anxiety: findings from a longitudinal twin study. Dev Psychopathol. 2022;34:1666–85.

46. Birn RM, Shackman AJ, Oler JA, Williams LE, McFarlin DR, Rogers GM, et al. Evolutionarily conserved prefrontal-amygdalar dysfunction in early-life anxiety. Mol Psychiatry. 2014;19:915–22.
47. Nair AB, Jacob S. A simple practice guide for dose conversion between animals and human. J Basic Clin Pharm. 2016;7:27–31.
48. Nair A, Morsy MA, Jacob S. Dose translation between laboratory animals and human in preclinical and clinical phases of drug development. Drug Dev Res. 2018;79:373–82.
49. Fox AS, Shelton SE, Oakes TR, Davidson RJ, Kalin NH. Trait-like brain activity during adolescence predicts anxious temperament in primates. PLoS One. 2008; 3:e2570.
50. Kecskemeti S, Samsonov A, Hurley SA, Dean DC, Field A, Alexander AL. MPnRAGE: a technique to simultaneously acquire hundreds of differently contrasted MPRAGE images with applications to quantitative T1 mapping. Magn Reson Med. 2015;75:1040–53.
51. Kecskemeti S, Samsonov A, Velikina J, Field AS, Turski P, Rowley H, et al. Robust motion correction strategy for structural mri in unsedated children demonstrated with three-dimensional radial MPnRAGE. Radiology. 2018;289:509–16.
52. Avants BB, Epstein CL, Grossman M, Gee JC. Symmetric diffeomorphic image registration with cross-correlation: Evaluating automated labeling of elderly and neurodegenerative brain. Med Image Anal. 2008;12:26–41.
53. Camino: Open-Source Diffusion-MRI Reconstruction and Processing – 02759.pdf [Internet]. Available from: https://afni.nimh.nih.gov/sscc/staff/rwcox/ISMRM_2006/ISMRM%202006%20-%203340/files/02759.pdf. Accessed 24 Jan 2021.
54. Zhang H, Yushkevich P, Alexander D, Gee J. Deformable registration of diffusion tensor MR images with explicit orientation optimization. Med Image Anal. 2006; 10:764–85.
55. Jenkinson M, Beckmann CF, Behrens TEJ, Woolrich MW, Smith SM. FSL. Neuroimage. 2012;62:782–90.
56. Brauer M, Curtin JJ. Linear mixed-effects models and the analysis of nonindependent data: a unified framework to analyze categorical and continuous independent variables that vary within-subjects and/or within-items. Psychol Methods. 2018;23: 389–411.
57. Cox RW. AFNI: software for analysis and visualization of functional magnetic resonance neuroimages. Comput Biomed Res. 1996;29:162–73.
58. Cherubini A, Péran P, Hagberg GE, Varsi AE, Luccichenti G, Caltagirone C, et al. Characterization of white matter fiber bundles with T2* relaxometry and diffusion tensor imaging. Magn Reson Med. 2009;61:1066–72.
59. Moody JF, Aggarwal N, Dean DC, Tromp DPM, Kecskemeti SR, Oler JA, et al. Longitudinal assessment of early-life white matter development with quantitative relaxometry in nonhuman primates. Neuroimage. 2022;251:118989.
60. Marisca R, Hoche T, Agirre E, Hoodless LJ, Barkey W, Auer F, et al. Functionally distinct subgroups of oligodendrocyte precursor cells integrate neural activity and execute myelin formation. Nat Neurosci. 2020;23:363–74.
61. Levine JM, Reynolds R, Fawcett JW. The oligodendrocyte precursor cell in health and disease. Trends Neurosci. 2001;24:39–47.
62. Crawford AH, Stockley JH, Tripathi RB, Richardson WD, Franklin RJM. Oligodendrocyte progenitors: adult stem cells of the central nervous system? Exp Neurol. 2014;260:50–5.
63. Fernandez-Castaneda A, Gaultier A. Adult oligodendrocyte progenitor cells – multifaceted regulators of the CNS in health and disease. Brain Behav Immun. 2016;57:1–7.
64. Clayton BLL, Tesar PJ. Oligodendrocyte progenitor cell fate and function in development and disease. Curr Opin Cell Biol. 2021;73:35–40.
65. Zhang SC, Ge B, Duncan ID. Adult brain retains the potential to generate oligodendroglial progenitors with extensive myelination capacity. Proc Natl Acad Sci. 1999;96:4089–94.
66. Deoni SCL. Quantitative relaxometry of the brain. Top Magn Reson Imaging. 2010;21:101–13.
67. O'Muircheartaigh J, Vavasour I, Ljungberg E, Li DKB, Rauscher A, Levesque V, et al. Quantitative neuroimaging measures of myelin in the healthy brain and in multiple sclerosis. Hum Brain Mapp. 2019;40:2104–16.
68. Kumar R, Nguyen HD, Macey PM, Woo MA, Harper RM. Regional brain axial and radial diffusivity changes during development. J Neurosci Res. 2012;90:346–55.
69. Winklewski PJ, Sabisz A, Naumczyk P, Jodzio K, Szurowska E, Szarmach A. Understanding the physiopathology behind axial and radial diffusivity changes—what do we know? Front Neurol. 2018;9:92.
70. Alexander AL, Lee JE, Lazar M, Field AS. Diffusion tensor imaging of the brain. Neurotherapeutics. 2007;4:1–14.
71. Kalin NH, Fox AS, Kovner R, Riedel MK, Fekete EM, Roseboom PH, et al. Overexpressing corticotropin-releasing factor in the primate amygdala increases anxious temperament and alters its neural circuit. Biol Psychiatry. 2016;80:345–55.
72. Furey ML, Drevets WC. Antidepressant efficacy of the antimuscarinic drug scopolamine: a randomized, placebo-controlled clinical trial. Arch Gen Psychiatry. 2006;63:1121–9.
73. Sipos ML, Burchnell V, Galbicka G. Dose-response curves and time-course effects of selected anticholinergics on locomotor activity in rats. Psychopharmacology 1999;147:250–6.
74. Scarr E. Muscarinic receptors: their roles in disorders of the central nervous system and potential as therapeutic targets. CNS Neurosci Ther. 2012;18:369–79.
75. Yamada M, Miyakawa T, Duttaroy A, Yamanaka A, Moriguchi T, Makita R, et al. Mice lacking the M3 muscarinic acetylcholine receptor are hypophagic and lean. Nature. 2001;410:207–12.
76. Cerghet M, Skoff RP, Swamydas M, Bessert D. Sexual dimorphism in the white matter of rodents. J Neurol Sci. 2009;286:76–80.
77. Yasuda K, Maki T, Kinoshita H, Kaji S, Toyokawa M, Nishigori R, et al. Sex-specific differences in transcriptomic profiles and cellular characteristics of oligodendrocyte precursor cells. Stem Cell Res. 2020;46:101866.
78. Swamydas M, Bessert D, Skoff R. Sexual dimorphism of oligodendrocytes is mediated by differential regulation of signaling pathways. J Neurosci Res. 2009; 87:3306–19.
79. Fox AS, Kalin NH. A translational neuroscience approach to understanding the development of social anxiety disorder and its pathophysiology. Am J Psychiatry. 2014;171:1162–73.

ACKNOWLEDGEMENTS

We thank Dr. Jason F. Moody for his expertize and assistance with the quantitative relaxometry analyses, and Carissa Boettcher for assisting with the animal care and experimentation protocols. We also thank the many other members of the staffs of the Harlow Center for Biological Psychology and Wisconsin National Primate Research Center. This work was supported by grants from the National Institutes of Health: R01-MH081884 (NHK); R01-MH046729 (NHK)—includes NIH Bench-to-Bedside supplement (Award ID: 654199; MAB, NHK); T32-GM140935 (NA); T32-MH018931 (NA). The funding sources played no role in the conceptualization, design, execution, or analysis of any part of the study.

AUTHOR CONTRIBUTIONS

NA, JAO, DPMT, PHR, MKR, VRE, MAB, and NHK all made substantial contributions to the conception or design of the work; or the acquisition, analysis, or interpretation of data for the work. NA and NHK drafted the work, and all authors contributed to critically revising the draft for important intellectual content and provided final approval of the version to be published. NA and NHK agree to be accountable for all aspects of the work in ensuring that questions related to the accuracy or integrity of any part of the work are appropriately investigated and resolved.

COMPETING INTERESTS

NHK reported receiving grants from the National Institute of Mental Health; consulting to CME Outfitters, the Pritzker Neuropsychiatric Disorders Research Consortium, the Skyland Trail Advisory Board, the Early Life Adversity Research External Scientific Advisory Board at the University of Texas at Austin, and Corcept Therapeutics Incorporated; and serving as editor-in-chief of The American Journal of Psychiatry during the conduct of the study. The other authors report no potential conflicts of interests.

ADDITIONAL INFORMATION

Supplementary information The online version contains supplementary material available at https://doi.org/10.1038/s41386-023-01686-1.

Correspondence and requests for materials should be addressed to Nakul Aggarwal.

Reprints and permission information is available at http://www.nature.com/reprints

Publisher's note Springer Nature remains neutral with regard to jurisdictional claims in published maps and institutional affiliations.